

A Formation Map of Iron-Containing Intermetallic Phases in Recycled Cast Aluminum Alloys



E. CINKILIC, C.D. RIDGEWAY, X. YAN, and A.A. LUO

The cooling rate-dependent modification effect of Mn on the formation of Fe-containing intermetallic phases during solidification of Al-Si-Mg secondary cast aluminum alloys [containing 0.5 to 1 pct Fe (All compositions are in wt pct unless otherwise stated.)] was investigated by CALPHAD modeling and solidification experiments. The critical Mn concentration required to prevent the formation of detrimental β -Al₅FeSi was found to be dependent on both the alloy composition (particularly the Fe/Mn ratio) and the cooling rate. A map of Fe/Mn ratio vs cooling rate was created, to summarize the metallurgical conditions of Fe-rich intermetallic phase formation. By understanding such formation conditions, the microstructure of aluminum castings can be controlled to create low-cost secondary alloys with high Fe content.

<https://doi.org/10.1007/s11661-019-05469-6>

© The Minerals, Metals & Materials Society and ASM International 2019

I. INTRODUCTION

THE demand for improved fuel economy and lower greenhouse gas emission without compromising passenger safety and performance has led to increased use of lightweight materials in vehicles over the last few decades.^[1] Such demand has made aluminum alloys the material of choice for many automotive applications because of their lightweight, good specific strength, and exceptional corrosion resistance.^[2] However, the high costs of primary aluminum production^[3] and component manufacturing often limit the widespread usage of aluminum in the vehicle design.^[4] To achieve further weight reduction in light vehicles while maintaining the affordability, it is essential to lower the manufacturing cost of aluminum components.

Aluminum can be recycled many times with exceptional recovery rates, where the energy required to produce secondary or recycled aluminum is only 5 pct of the energy used in the production of primary aluminum.^[3] Such a reduction highlights strong economic and environmental benefits of utilizing recycled aluminum in production of parts for automotive industry.^[3] Additionally, the excellent castability of aluminum

alloys, especially of the Al-Si based alloys, enables the production of complex components as well as the consolidation of welded or joined subsystems into a single cast part at a lower cost.^[2]

Despite the promising outlook for the use of secondary aluminum, there is a cascade effect from continued recycling of aluminum, *i.e.*, accumulation of alloying/impurity elements such as Fe, Mg, Cu, Zn, *etc.*, due to the difficulty in removing them in the recycling process.^[5,6] The result is that the properties of the recycled aluminum alloys can be significantly altered by the excess concentrations of these elements and renders the recycled material ill-suited for safety critical applications.

Of all impurity elements, Fe is considered the most detrimental, and its deleterious effect on the mechanical properties of Al-Si alloys is well known to the aluminum casting industry.^[7-9] Fe can form numerous intermetallic phases, such as, θ -Al₁₃Fe₄, α -Al₈Fe₂Si, β -Al₅FeSi, δ -Al₄FeSi₂, π -Al₈FeMg₃Si₂, *etc.*, when it is combined with other alloying elements. The size, morphology, and volume fraction of these Fe-containing intermetallics have a pronounced effect on the as-cast mechanical properties of Al-Si alloys. The most common and detrimental Fe-containing intermetallic observed in hypoeutectic Al-Si casting alloys is β -Al₅FeSi phase which forms as interconnected thin platelets with a needle-like appearance in a polished cross-section.^[10-12] The sharp tips of these platelets act as stress concentrators under loading and reduce the alloy ductility, rendering these alloys unusable for structural components. Therefore, it is imperative to prevent the formation of β -Al₅FeSi in alloys used for applications where ductility is essential.^[13-15]

E. CINKILIC and C.D. RIDGEWAY are with the Department of Materials Science & Engineering, The Ohio State University, Columbus, OH 43210. X. YAN is with the Alcoa Technical Center, New Kensington, PA 15068. A.A. LUO is with the Department of Materials Science & Engineering, The Ohio State University and also with the Department of Integrated Systems Engineering, The Ohio State University, Columbus, OH 43210. Contact e-mail: luo.445@osu.edu

Manuscript submitted June 21, 2019.

The formation of detrimental β -Al₅FeSi phase can be suppressed in several ways. The commonly employed ones are either rapid solidification at high cooling rates to promote the formation of α -Al₈Fe₂Si phase or by adding Mn to promote the formation of α -Al₁₅(Fe,Mn)₃Si₂ phase.^[7-9,16] In addition, it was also demonstrated that the thermal history of molten alloy (*i.e.*, superheat, holding time) can alter the solidification path and result in the formation of α -Al₈Fe₂Si phase under non-equilibrium cooling conditions.^[17] Both α -Al₈Fe₂Si and α -Al₁₅(Fe,Mn)₃Si₂ can form in the so-called “Chinese-script” morphology or as compact globular particles, which are considered less detrimental to the mechanical properties.^[8] The crystal structure, typical morphology, and their relative effect on ductility of Al-Si-Mg alloys of these Fe-containing intermetallics are given in Table I.

The established standard to mitigate the adverse effects of Fe on the mechanical properties of cast aluminum alloys, regardless of cooling conditions, is to maintain a manganese concentration that is at least the half of the iron, if the iron content exceeds 0.45 pct.^[7] However, the critical Mn content to eliminate β -Al₅FeSi phase depends not only on the alloy composition but the cooling rate as well.^[19,20] Several studies on the modification effect of Mn and cooling rate on Fe-containing intermetallic phases have been reported for various alloy systems.^[21-23] An increased cooling rate will generally suppress the formation of β -Al₅FeSi and promote the formation of non-equilibrium α -Al₈Fe₂Si in coexistence of α -Al₁₅(Fe,Mn)₃Si₂. In general, the volume fraction of Fe-containing intermetallics must be minimal, since they are hard and brittle and negatively influence the

mechanical properties of the alloy. Therefore, it is important to determine the critical Mn content which minimizes α -Al₁₅(Fe,Mn)₃Si₂ phase fraction and avoids sludge formation, yet ensures the elimination of β -Al₅FeSi. Further, this compositional effect must be matched with the kinetics incorporated in the cooling rate effect of eliminating the β -Al₅FeSi.

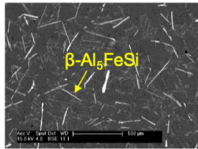
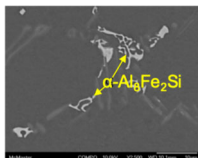
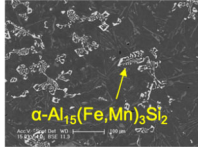
In this study, the cooling rate-dependent Fe-to-Mn ratio critical to β -Al₅FeSi phase formation in high Fe-content (0.5, 0.7, and 1.0 pct) Al-Si-Mg-Fe-Mn alloys was systematically investigated using CALculation of PHase Diagram (CALPHAD) modeling and solidification experiments. The aim of the study was to establish a comprehensive map on the formation for Fe-containing intermetallics in recycled aluminum alloys with high Fe contents. The formation map, in which both alloy composition and cooling rate were considered, can serve as a guide to minimize the Fe-containing intermetallic formation across all major casting processes, *i.e.*, sand casting, permanent mold casting, and high-pressure die casting (HPDC).

II. MATERIALS AND METHODS

A. Thermodynamic Modeling

CALculation of PHase Diagrams (CALPHAD) is a powerful tool that allows virtual investigation of phase equilibria and can guide the design of critical experiments for accelerated optimization of complex microstructures of multi-component alloy systems.^[24] The CALPHAD modeling of Al-Si-Mg-Fe-Mn quinary system was carried out using PandatTM software by

Table I. The Morphology of Fe-Containing Intermetallics Directly Affect the Ductility of the Al-Si-Mg Alloys

Fe-Rich Intermetallic	Crystal Structure	Morphology	Ductility Loss
β -Al ₅ FeSi	monoclinic ^[18] (platelets)		severe
α -Al ₈ Fe ₂ Si	hexagonal ^[18] (Chinese script)	 [16]	less severe
α -Al ₁₅ (Fe,Mn) ₃ Si ₂	cubic ^[18] (Chinese script)		less severe

CompuTherm LLC. (Madison, WI). The thermodynamic descriptions of investigated phases are detailed in PanAl2018 thermodynamic and mobility database.

The effect of Mn content on the alloy microstructure was investigated under equilibrium and non-equilibrium conditions for the composition ranges of 7 to 10 pct Si, 0.3 to 0.5 pct Mg, 0.1 to 1.3 pct Mn, and 0.1 to 1.3 pct Fe. The investigated composition ranges were selected to cover most of the heat-treatable hypoeutectic Al-Si casting alloys that are used in a wide variety of casting applications.

The isopleths (vertical sections) of the Al-Si-Mg-Fe-Mn system were calculated for fixed concentrations of Si, Mg, and Fe, but Mn varied to determine the thermodynamic stability range of β -Al₅FeSi phase. Based on phase equilibrium calculations, the high-throughput solidification calculations (HTSC) were performed using both Lever rule (equilibrium) and Scheil solidification (assuming complete mixing in liquid but no diffusion in solid) models to determine the critical Mn contents that can eliminate the β -Al₅FeSi phase within the aforementioned compositional space, which was probed by compositional step sizes of 1, 0.1, 0.1 pct for Si, Mg, and Fe, respectively. For every combination of compositions, the Mn content was varied by 0.01 pct to determine the minimum Mn content required to suppress β -phase formation.

B. Materials and Melt Preparation

Target alloy compositions with various Fe-to-Mn ratios were selected based on CALPHAD calculations. Commercially pure aluminum (CP Al) and master alloys of Al-12 pct Si, Al-10 pct Fe, Al-25 pct Mn, and Al-68 pct Mg were used to prepare the alloys. The compositions of CP Al and master alloys are presented in Table II. The excess Fe that can be introduced into prepared alloys through CP Al and other master alloys was considered in the mass balance calculations of prepared alloys. The alloys were melted in graphite crucibles using an induction furnace. Alloying materials and crucibles were pre-heated in an electric resistance furnace at 200 °C for 10 minutes prior to melting. Then, the materials were heated up to 750 °C and held at this temperature for 30 minutes.

The compositional analysis on prepared alloys was performed using a SPECTROMAXx M Bench Top optical emission spectrometer (wavelength range 140 to 670 nm) to ensure that target compositions are obtained. The measured compositions of selected alloys are given in Table III.

C. Casting Processes and Cooling Curve Analysis

After melting, alloys were cooled at different rates to test the effect of cooling conditions on the alloy microstructure. The cooling curve analysis (CCA) or thermal analysis (TA) is used to determine critical arrest temperatures during solidification. The cooling curves were measured using ungrounded and exposed K-type thermocouples for faster response and a National Instruments NI-9217 data acquisition system which

Table II. Measured Chemical Composition of Commercially Pure Aluminum and Master Alloys Used in this Study

Master Alloy	Si	Fe	Mn	Mg	Cu	Al
CP Al	0.02	0.04	—	—	—	bal.
Al-Si	11.8	0.2	—	—	0.03	bal.
Al-Fe	0.07	9.71	0.04	0.01	0.05	bal.
Al-Mn	0.2	0.2	24.6	—	—	bal.
Al-Mg	0.1	0.15	—	67.75	—	bal.

Table III. Measured Chemical Compositions of Selected Prepared Alloys

Alloy	Si	Mg	Fe	Mn	Al
Al-8Si-0.35Mg-0.5Fe-0.3Mn	8.14	0.37	0.52	0.33	bal.
Al-8Si-0.35Mg-0.5Fe-0.4Mn	8.18	0.36	0.48	0.4	bal.
Al-8Si-0.35Mg-0.5Fe-0.5Mn	8.02	0.38	0.53	0.51	bal.
Al-8Si-0.35Mg-0.7Fe-0.0Mn	8.49	0.37	0.74	0.007	bal.
Al-8Si-0.35Mg-0.7Fe-0.5Mn	8.02	0.34	0.73	0.48	bal.
Al-8Si-0.35Mg-0.7Fe-1.0Mn	8.14	0.39	0.71	0.98	bal.
Al-8Si-0.35Mg-1.0Fe-0.4Mn	8.32	0.35	0.97	0.42	bal.
Al-8Si-0.35Mg-1.0Fe-0.6Mn	8.24	0.34	1.03	0.61	bal.
Al-8Si-0.35Mg-1.0Fe-1.2Mn	8.22	0.37	1.01	1.15	bal.

allows simultaneous data collection on four (4) channels. The cooling curves were recorded at a rate of 50 data points per second. Alloys were poured into standard cooling cups which are made of no-bake sand and equipped with a K-type thermocouple. The standard cooling cups are ideal to study microstructures that can be observed in sand castings under relatively slow cooling conditions. To investigate the effect of higher cooling rates on the Fe-to-Mn ratio and resulting microstructure, rod castings and wedge castings were produced. The dimensions of these castings and locations of thermocouples within the castings are provided in Figures 6 and 7 along with microstructural images obtained from these castings. The 1st and 2nd derivatives of the cooling curves were calculated to capture important arrest points, such as primary Al formation, eutectic silicon formation, Fe-containing intermetallic formation. The derivative curves were smoothed using locally estimated scatterplot smoothing (LOESS) method. The overall cooling rate at a given location was calculated based on the time difference between the start of aluminum dendrite formation (liquidus temperature) and the end of solidification (solidus temperature) as determined from the 2nd derivative of the cooling curves $((T_{\text{liquidus}} - T_{\text{solidus}})/(t_{\text{liquidus}} - t_{\text{solidus}}))$. Thus, the cooling rates were determined to be 0.4 °C/s for sand cooling cup castings, ~ 30 °C/s for rod castings and ~ 65 °C/s, 5 °C/s, 2 °C/s, 1.5 °C/s for selected locations in the wedge castings.

D. Microstructural Characterization

The microstructure of the specimens was investigated using both optical and electron microscopy. The specimens were polished following standard metallographic procedures and then selectively etched using a 0.74 pct

HF solution to distinguish Fe-rich intermetallic phases in optical microscopy investigations. The microstructure characterization of the samples and compositional analysis of intermetallics were carried out using a FEI/Philips XL-30 scanning electron microscope (SEM) equipped with an energy-dispersive spectroscopy (EDS) system. The samples were re-polished with colloidal silica to remove the etched layer on the Fe-containing intermetallics for accurate compositional analysis. The back-scattered images of the samples and EDS analysis on intermetallic phases were obtained under an accelerating voltage of 15 kV.

III. RESULTS AND DISCUSSION

A. CALPHAD Simulations

The Fe-to-Mn ratio critical to β -phase formation was first investigated under equilibrium conditions. To examine the thermodynamic stability range of β -phase as a function of temperature and Mn concentration, equilibrium isopleths were calculated for varying levels of Si, Mg, and Fe. Figure 1(a) shows an isopleth calculated for Al-8 pct Si-0.35 pct Mg-0.6 pct Fe, which maps the equilibrium phase constituents for different Mn concentrations within the temperature range of 25 °C to 700 °C. The α -Al₁₅(Fe,Mn)₃Si₂ phase becomes stable when Mn is above 0.022 pct at 566 °C. A boundary separates the domain of “ α -Al + Si + β -Al₅FeSi + α -Al₁₅(Fe,Mn)₃Si₂ (red area)” from “ α -Al + Si + α -Al₁₅(Fe,Mn)₃Si₂ (blue area)” and intersects the solidus line (566 °C) at 0.58 pct Mn. The isopleths for different Mg and Si concentrations of the same Fe level (0.6 pct) are presented in Figures 1(b) and (c). The increase in Mg reduces the solidus temperature from 566 °C to 561 °C, while the Mn concentration that bisects the solidus line slightly decreases from 0.58 to 0.576 pct as shown in Figure 1(b). On the other hand, the influence of Si concentration on the solidus temperature and intersecting Mn concentration is minimal according to the equilibrium calculations (Figure 1(c)).

A small set of calculated equilibrium solidification paths for different levels of Fe are shown in Figure 1(d) as an example. In Figure 1(e), the variation of total phase fraction of both β - and α -phases with Mn content for a fixed alloy composition of Al-8 pct Si-0.35 pct Mg-0.6 pct Fe is presented. Mn concentration of 0.59 pct is enough to inhibit the formation of β -phase under equilibrium solidification conditions for 0.6 pct Fe. A composition map was generated by plotting critical Mn contents, which are extracted through the analysis of HTC results, against the associated Fe level (Figure 1(f)). The critical Fe-to-Mn ratio is determined to be ~ 1 for equilibrium conditions and the ratio of 1 holds valid if the Si and Mg concentrations were varied within the investigated composition range.

Following the HTC calculations for equilibrium cooling conditions, Scheil solidification simulations were performed to determine critical Mn content under non-equilibrium cooling conditions using HTC function of Pandat. Total phase fraction of Fe-containing

intermetallics as a function of Mn content for Al-8 pct Si-0.35 pct Mg-0.6 pct Fe under non-equilibrium cooling conditions is shown in Figure 2(a). The Mn concentration required to eliminate β -phase is determined to be 1.16 pct for 0.6 pct Fe, which is almost two times higher than the critical Mn content required to eliminate β -phase under equilibrium cooling conditions. Fe-to-Mn ratio critical to β -phase formation varies between ~ 0.4 and 0.6 (Figure 2(b)) within the investigated composition range for non-equilibrium conditions. The simulation results imply that critical Mn content must be higher than Fe concentration to eliminate the β -phase at high cooling rates, which contradicts with the literature.^[7]

B. Casting Experiments

To validate the modeling results for equilibrium and non-equilibrium cooling conditions, alloys of different Fe levels were prepared with varying Fe-to-Mn ratios. The back-scattered SEM images of alloys with 0.7 pct Fe that were cooled at a rate of ~ 0.4 °C/s in a standard sand cooling cup are presented in Figure 3. As predicted by the equilibrium CALPHAD calculations, the Fe-to-Mn ratio of ~ 1 , completely suppresses the formation of β -Al₅FeSi phase and the same ratio holds for the alloys with 0.5, 0.7, and 1 pct Fe as well. The CCA clearly shows that the peak associated with formation of β -Al₅FeSi phase in the 2nd derivative of cooling curve vanishes from the alloy with the Fe-to-Mn ratio of ~ 1 (Figure 4). The start temperature of β -Al₅FeSi phase formation was suppressed with the Mn addition, which can be easily discerned from the cooling curves shown in Figure 4. The liberated latent heat from the β -Al₅FeSi phase formation manifested itself as a knee in the cooling curves of alloys containing 0.25 and 0.5 pct Mn. However, the formation start temperature of β -Al₅FeSi phase for the alloy that does not contain any Mn was not observed. This was attributed to greater release of latent heat of primary Al dendrites compared to the heat of formation associated with the β -Al₅FeSi phase. Due to the close proximity of the transformation temperatures which are only ~ 5 C apart according to the equilibrium solidification simulation, the β -Al₅FeSi formation could not be distinguished from that of the primary Al dendrites when no Mn was present.

According to the equilibrium solidification calculations, the formation of β -Al₅FeSi begins after the formation of aluminum dendrites and continues during the eutectic transformation in alloys with 0.7 pct Fe (Figure 5). However, the primary or pre-dendritic β -Al₅FeSi phase is present in alloy without Mn (Figure 3(a)) which has been attributed to heterogeneous nucleation and growth of primary β -Al₅FeSi on oxide-bifilms as suggested by Cao and Campbell.^[25] The size and volume fraction of pre-eutectic β -Al₅FeSi can be limited with an increased level of Mn content (Figures 2(b) and (c)), which suppressed the formation temperature from pre-dendritic to temperatures closer to the eutectic transformation as determined from CCA. The addition of 0.25 pct Mn changes the equilibrium solidification path and α -Al₁₅(Fe,Mn)₃Si₂ phase

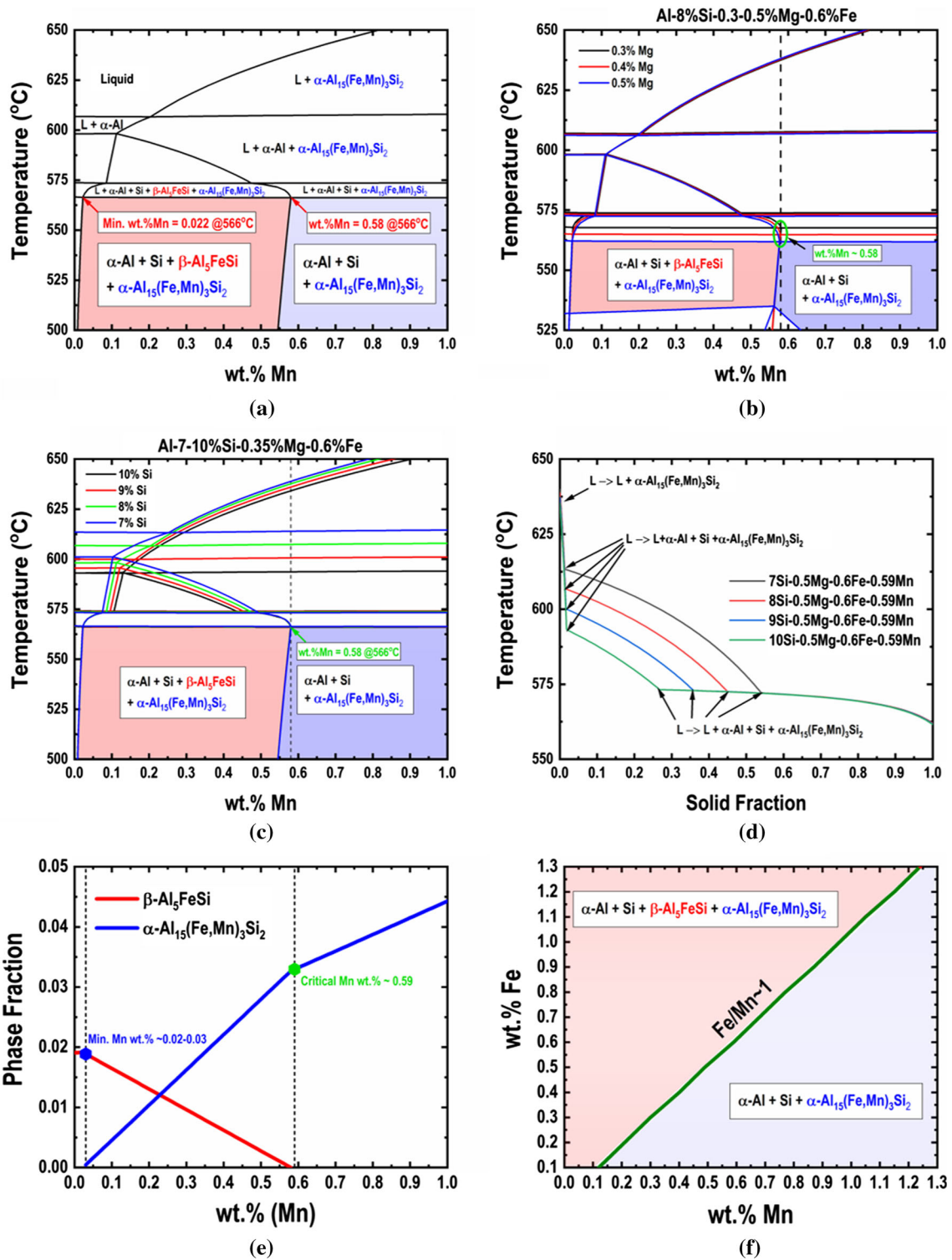


Fig. 1—(a) Isoleth for Al-8 pct Si-0.35 pct Mg-0.6 pct Fe showing equilibrium phase constituents; (b) and (c) the effect of Mg and Si content on the equilibrium phase stability; (d) calculated equilibrium solidification paths; (e) the change in total phase fraction of Fe-containing intermetallics with Mn concentration for Al-8 pct Si-0.35 pct Mg-0.6 pct Fe; and (f) the effect of Fe and Mn content on the formation of β -Al₅FeSi intermetallic phase for composition ranges of 7 to 10 pct Si, 0.35 to 0.5 pct Mg, 0.1 to 1.3 pct Mn, 0.1 to 1.3 pct Fe.

becomes the primary solidification product and continues to form through eutectic reactions with other stable phases. The α -Al₁₅(Fe,Mn)₃Si₂ with coarse polyhedral (primary phase) or with Chinese-script

morphology was observed in all of Mn-containing alloys. It must be noted that the α -Al₁₅(Fe,Mn)₃Si₂ phase was significantly refined when the Mn content increased from 0.75 to 1 pct (Figure 2(e)). This was also

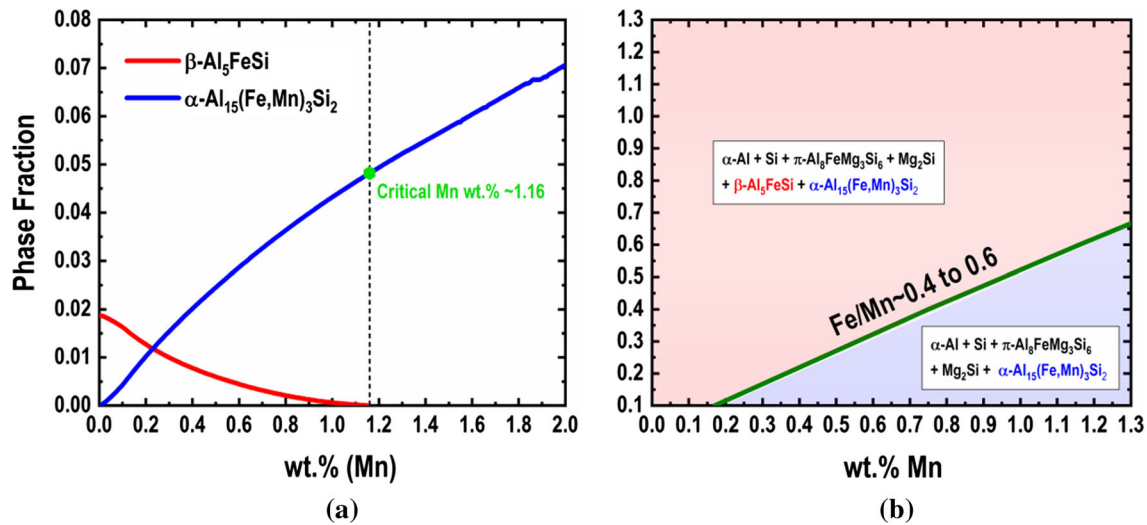


Fig. 2—(a) The change in total phase fraction of Fe-containing intermetallics with Mn concentration for Al-8 pct Si-0.35 pct Mg-0.6 pct Fe; and (b) the effect of Fe and Mn content on the formation of $\beta\text{-Al}_5\text{FeSi}$ intermetallic phase for composition ranges of 7 to 10 pct Si, 0.35-0.5 pct Mg, 0.1 to 1.3 pct Mn, 0.1 to 1.3 pct Fe.

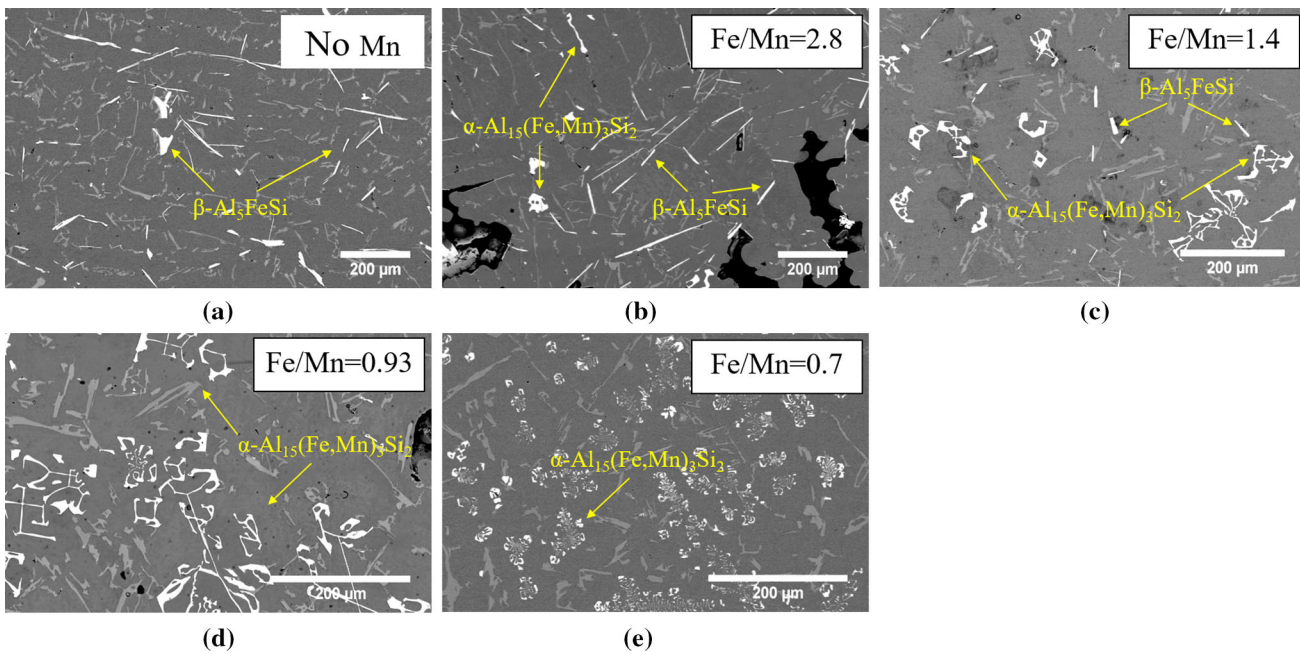


Fig. 3—Back-scattered SEM images of Al-8 pct Si-0.35 pct Mg alloys solidified in standard cooling cups, (a) 0.7 pct Fe-0 pct Mn; (b) 0.7 pct Fe-0.25 pct Mn; (c) 0.7 pct Fe-0.5 pct Mn; (d) 0.7 pct Fe-0.75 pct Mn; and (e) 0.7 pct Fe-1 pct Mn.

observed in secondary aluminum castings produced by HPDC^[15] and the refinement was attributed to increased nucleation of $\alpha\text{-Al}_{15}(\text{Fe},\text{Mn})_3\text{Si}_2$ phase due to enlarged undercooling as a result of increase in liquidus temperature with higher Mn content.

The chemical compositions of intermetallic phases observed in prepared alloys and cooled in sand cooling cups are presented in Table IV. In contrast with the CALPHAD calculations that suggest very limited Mn solubility in $\beta\text{-Al}_5\text{FeSi}$ phase, the EDS analyses revealed that large amount of Mn was dissolved in this phase.

The Mn solubility in $\beta\text{-Al}_5\text{FeSi}$ phase was previously reported by Kral.^[18] However, Kral's reported solubility limit of 0.5 at. pct is well below the measured value of 2.42 at. pct in this study. On the other hand, the EDS analysis results on the $\beta\text{-Al}_5\text{FeSi}$ phase in alloys without Mn are in good agreement with CALPHAD calculations which suggests sand cooling cup experiments are good representative of equilibrium cooling conditions. The measured chemical composition of $\alpha\text{-Al}_{15}(\text{Fe},\text{Mn})_3\text{Si}_2$ phase is in good agreement with the CALPHAD calculations as well.

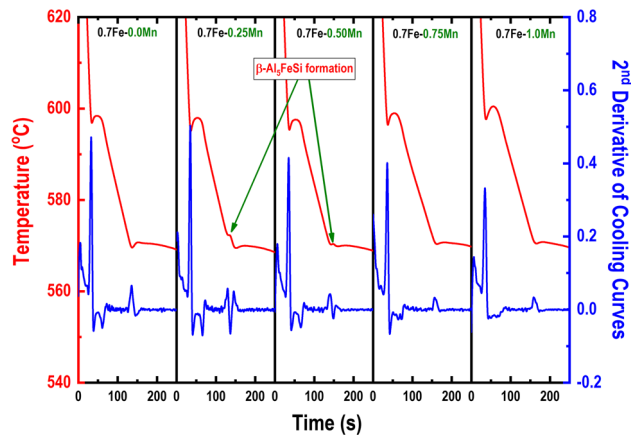


Fig. 4—Cooling curves of Al-8 pct Si-0.35 pct Mg-0.7 pct Fe alloys with varying levels of Mn (red lines) obtained from sand cooling cup experiments (0.4 °C/s) and second derivative of each cooling curve (Color figure online).

As previously stated, the formation of Fe-containing intermetallics is complicated by superheat, cooling rate, and alloy composition. Depending on the casting parameters, it is possible to obtain a variety of Fe-containing intermetallics with different composition and morphology in the as-cast microstructure of Al-Si alloys. In Figure 6, back-scattered SEM images of Al-8 pct Si-0.35 pct Mg-1 pct Fe with 0.4, 0.6, 0.8, and 1.2 pct Mn were cooled at a rate of ~ 30 °C/s. The Fe-containing intermetallics observed in 0.4 and 0.6 pct Mn were formed through a eutectic reaction simultaneously with Si phase interdendritically. The compositional analysis of phases with refined Chinese-script morphology is presented in Table V. The comparison between CALPHAD calculations and EDS results reveals that intermetallic phases were identified as α -Al₈Fe₂Si and α -Al₁₅(Fe,Mn)₃Si₂. Increasing Mn concentration to 0.8 pct led to the formation of intermetallics with needle-like morphology, which were identified as β -Al₅FeSi phase (Table V). The further increase of Mn content (1.2 pct) significantly increased β -Al₅FeSi phase fraction and resulted in the separation of Fe-containing intermetallic phases in the form of islands of α -Al₁₅(Fe,Mn)₃Si₂ phase-rich regions surrounded by β -Al₅FeSi phase regions. To further study the effect of cooling rate on Fe-to-Mn ratio, wedge castings and associated microstructure for Al-8 pct Si-0.35 pct Mg-0.7 pct Fe-0.25 pct Mn alloy are presented in Figure 7(b) as an example. β -Al₅FeSi phase is present in the microstructure at the slowly cooled regions of the wedge casting. However, 0.25 pct Mn is enough to suppress the formation of β -Al₅FeSi phase even at the cooling rate of 5 °C/s. A set of microstructure images of 0.7 pct Fe level for different cooling rates are presented in Figure 8. As observed in the case of rod casting samples, the increased concentration of Mn leads to the formation of β -Al₅FeSi phase formation at high cooling rates while it completely suppressed its formation at slower cooling rates.

C. A Formation Map of Fe-Containing Intermetallics

The simulation and experimental results in this study were summarized as a two-dimensional map, shown in Figure 9, correlating the cooling rate and Fe-to-Mn ratio to the intermetallics formed in the as-cast microstructure. The produced map is a guide for three different levels of Fe 0.5, 0.7, and 1 pct, and indicates that β -Al₅FeSi can only be eliminated under certain cooling conditions for specific Fe-to-Mn ratios. The two-dimensional map was shown to have three distinct zones, as indicated in Figure 9. In Zone 1, where the Fe-to-Mn ratio is equal to or less than 1 (higher Mn content than Fe) and the cooling rate ranged from 0.4 to 5 °C/s, the only Fe-rich intermetallic observed in the as-cast microstructure was α -Al₁₅(Fe,Mn)₃Si₂ phase which has less detrimental effect on the as-cast mechanical properties. The relatively slow cooling conditions and high Mn content led to the formation of thermodynamically stable α -Al₁₅(Fe,Mn)₃Si₂ phase, with only a change in the morphology of the intermetallic phase from well-known Chinese-script morphology to a refined polyhedrons. Most of the Fe is accommodated in the α -Al₁₅(Fe,Mn)₃Si₂, while Mn remains in the solid aluminum due to its high solubility. Therefore, at slow and intermediate cooling rates, Fe-to-Mn ratio must be 1 or lower (more Mn than Fe) to maintain a critical content of Mn in solidifying liquid that forces thermodynamic stability of α -Al₁₅(Fe,Mn)₃Si₂ phase, which preferentially consumes Fe over the β -Al₅FeSi phase. Otherwise, as in the high Fe-to-Mn ratio region of Zone 2 (more Fe than Mn), a mixture of β -Al₅FeSi and α -Al₁₅(Fe,Mn)₃Si₂ phases in the as-cast microstructure was observed at slow cooling rates which cause a loss in alloy ductility. This mixture remains undesirable as even small amounts of β -Al₅FeSi can degrade mechanical properties.

In Zone 3, where Fe-to-Mn ratio is equal to or higher than 1.6 for high cooling rates, non-equilibrium α -Al₈Fe₂Si and stable α -Al₁₅(Fe,Mn)₃Si₂ phases coexist in the as-cast microstructure with compact morphology. Fe and Si are rejected from the solidifying Al, which causes the solidifying liquid to contain high concentrations of Fe and Si at the solid-liquid interface. Since the diffusion of Fe from the solid/liquid interface into the bulk liquid is extremely slow, Fe solute at the solidification front builds up, which causes a local inhomogeneity.^[26] Because of this local compositional inhomogeneity, θ -Al₁₃Fe₄ phase becomes thermodynamically stable and nucleates. After nucleation of θ phase, it evolves into α -Al₈Fe₂Si and β -Al₅FeSi sequentially through a peritectic reaction during the solidification.^[16] At high cooling rates, it is possible to arrest the α -Al₈Fe₂Si phase, before it transforms into the β -Al₅FeSi phase. To observe this peritectic reaction, an alloy with high Fe concentration (Al-8Si-10Fe-0.35Mg) is prepared and solidified at cooling rates of 0.4 °C/s and 30 °C/s, respectively. The back-scattered SEM images of Fe-rich intermetallics that undergo the peritectic transformation are presented in Figure 10. When the cooling rate increased from 0.4 °C/s to 30 °C/s, the most outer layer of intermetallic (Al_{6.3}FeSi_{1.5}) observed in

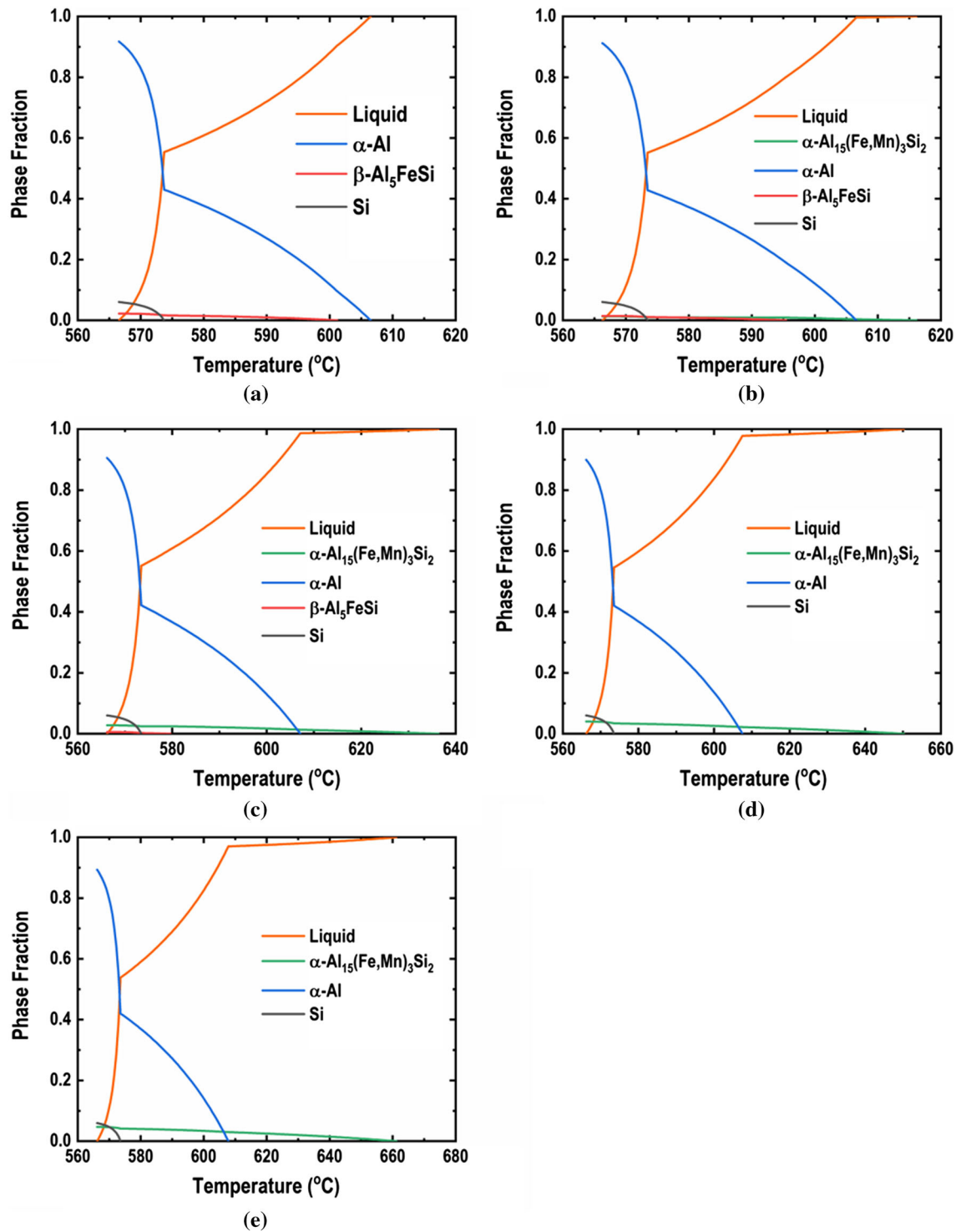


Fig. 5—Calculated phase fractions of Al-8 pct Si-0.35 pct Mg alloys solidified in standard cooling cups, (a) 0.7 pct Fe-0 pct Mn; (b) 0.7 pct Fe-0.25 pct Mn; (c) 0.7 pct Fe-0.5 pct Mn; (d) 0.7 pct Fe-0.75 pct Mn; and (e) 0.7 pct Fe-1 pct Mn.

Figure 10(a) did not form (Figure 10(b)) and the peritectic transformation was terminated at the $\text{Al}_{7.96}\text{Fe}_{1.3}\text{Si}$ layer due to a shorter solidification time. On the other hand, increasing Mn content did not inhibit the $\beta\text{-Al}_5\text{FeSi}$ phase formation at high cooling rates as expected (shown in Figure 9), but instead promoted the formation of very-fine $\beta\text{-Al}_5\text{FeSi}$ phase particles,

surrounding isolated $\alpha\text{-Al}_{15}(\text{Fe,Mn})_3\text{Si}_2$ islands. Even though $\alpha\text{-Al}_{15}(\text{Fe,Mn})_3\text{Si}_2$ is thermodynamically stable, in order to consume the remaining Fe to its structure, Fe diffusion is required. Since Fe diffusion is sluggish in both solid and liquid Al, it is not possible to transfer all the Fe in $\alpha\text{-Al}_{15}(\text{Fe,Mn})_3\text{Si}_2$ phase during rapid cooling. In addition, Fe segregation is increased due to higher

Table IV. Measured and Theoretical Compositions of Fe-Containing Intermetallics From Sand Cooling Cup Castings

Phase	Morphology		Al (At. Pct)	Si (At. Pct)	Fe (At. Pct)	Mn (At. Pct)
β -Al ₃ FeSi*	needle	measured	64.63	19.12	14.92	0.03
		CALPHAD	66.5	18.3	15.2	0.003
β -Al ₃ FeSi**	needle	measured	65.04	19.26	13.04	2.12
		CALPHAD	66.5	18.3	15.2	0.003
α -Al ₁₅ (Fe,Mn) ₃ Si ₂	Chinese-script /polyhedral	measured	69.85	11.08	10.56	7.65
		CALPHAD	70.5	12.1	8.9	8.5

*The composition of β -Al₃FeSi phase in alloy that contains no Mn.

**The composition of β -Al₃FeSi phase in alloys that contains Mn.

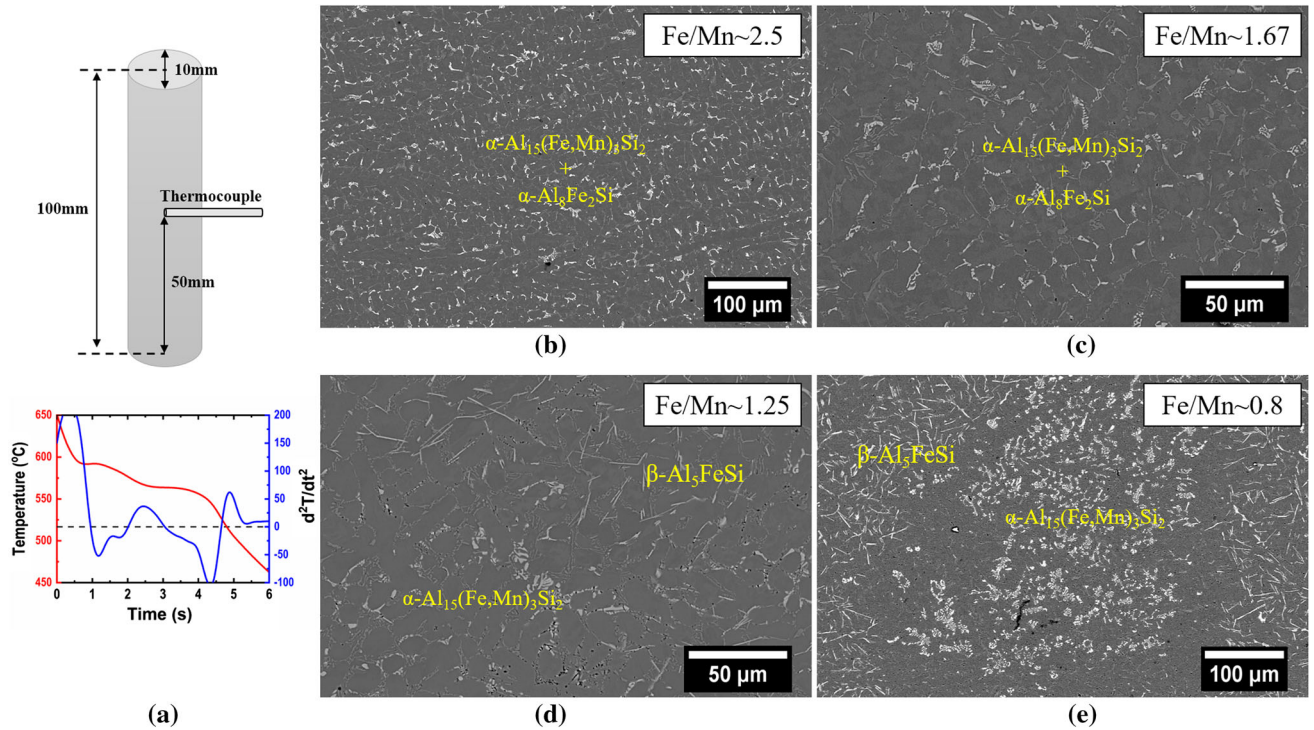


Fig. 6—(a) Schematic of rod castings and an example cooling curve obtained, Back-scattered SEM images of Al-8 pct Si-0.35 pct Mg-1 pct Fe, (b) 0.4 pct Mn, (c) 0.6 pctMn, (d) 0.8 pct Mn, (e) 1.2 pct Mn, cooled at a rate of ~ 30 °C/s.

Table V. Measured and Theoretical Compositions of Fe-Containing Intermetallics From Rod Castings

Phase	Morphology		Al (At. Pct)	Si (At. Pct)	Fe (At. Pct)	Mn (At. Pct)
α -Al ₃ Fe ₂ Si	refined Chinese script	measured	74.65	10.4	12.28	—
		CALPHAD	70	10.95	19	—
β -Al ₃ FeSi	needle	measured	72.93	19.69	4.63	2.76
		CALPHAD	66.5	18.3	15.2	0.003
α -Al ₁₅ (Fe,Mn) ₃ Si ₂	refined Chinese script	measured	74.34	10.51	9.24	5.91
		CALPHAD	70.5	12.1	8.9	8.5

content of Mn dissolved in the solid aluminum, which dramatically increases the Fe built-up at liquid/solid interface. Therefore, the peritectic reaction that occurs at a higher cooling rate will lead to the formation of fine β -Al₃FeSi phase particles.

The formation map presented in this study suggests that Fe-to-Mn ratio that favors the formation of less detrimental α -Al₁₅(Fe,Mn)₃Si₂ phase is cooling rate dependent. As previously mentioned, the established industry standard is to maintain Fe-to-Mn ratio of 2, if

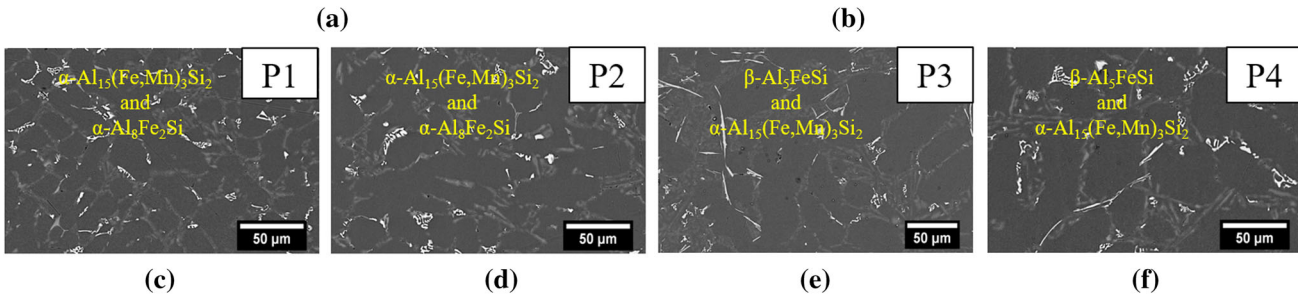
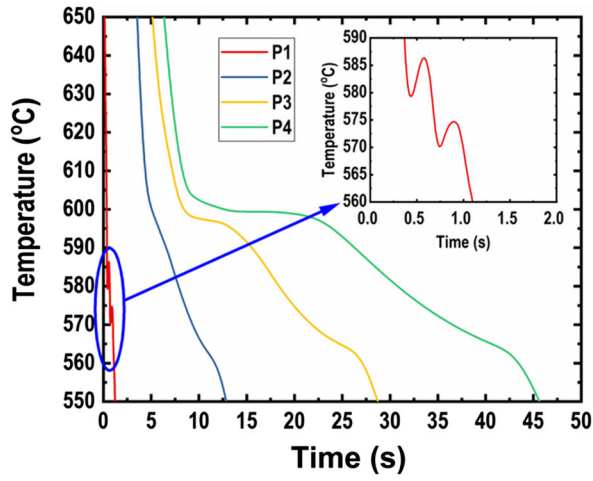
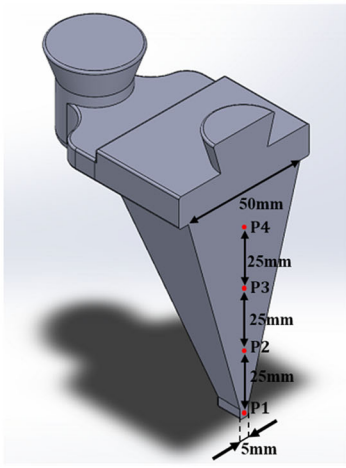


Fig. 7—(a) Cross-sectional view of wedge casting and locations of thermocouples; (b) recorded cooling curves for Al-8 pct Si-0.35 pct Mg-0.7 pct Fe-0.25 pct Mn alloy; (c) back-scattered SEM image from location P1 (~ 65 °C/s); (d) back-scattered SEM image from location P2 (~ 5 °C/s); (e) back-scattered SEM image from location P3 (~ 2 °C/s); (f) back-scattered SEM image from location P4 (~ 1.5 °C/s).

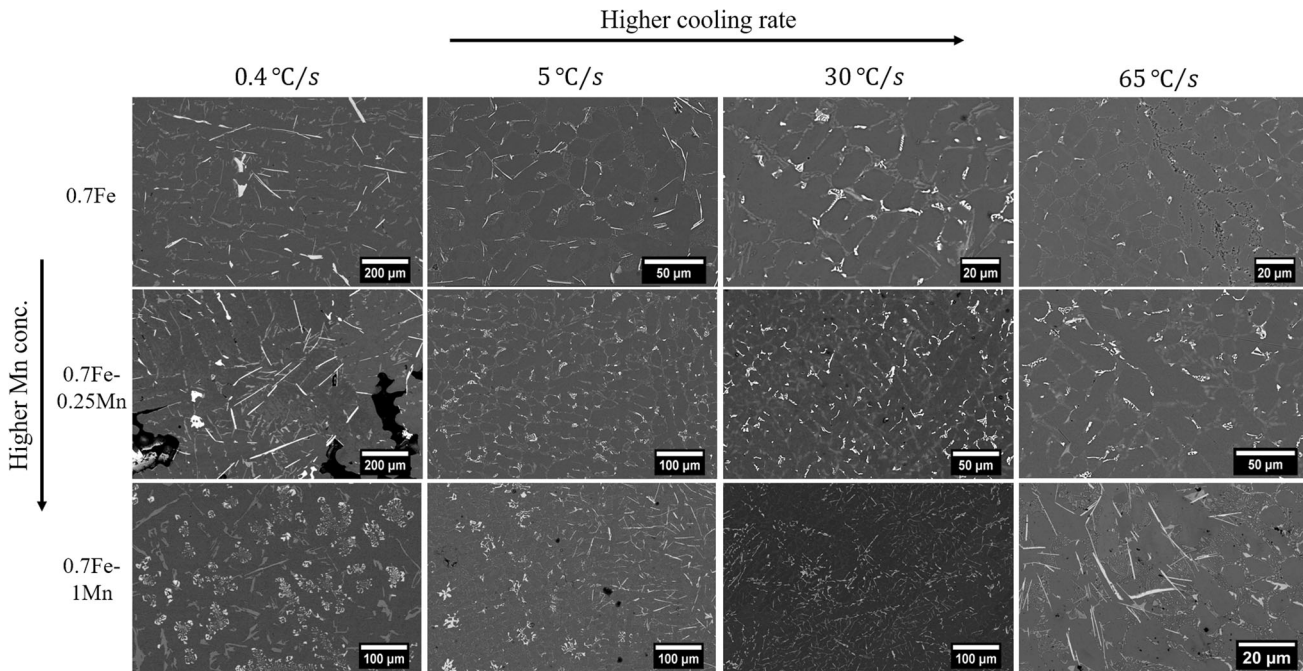


Fig. 8—Back-scattered SEM images showing effect of cooling rate and Fe/Mn ratio on the microstructure.

the Fe concentration exceeds 0.45 pct regardless of the cooling conditions.^[7] The purpose of suggested ratio is not complete elimination of β -Al₅FeSi phase from

microstructure, but rather reducing the average size of it by pushing its formation start temperature closer to the eutectic solidification temperature. However, the

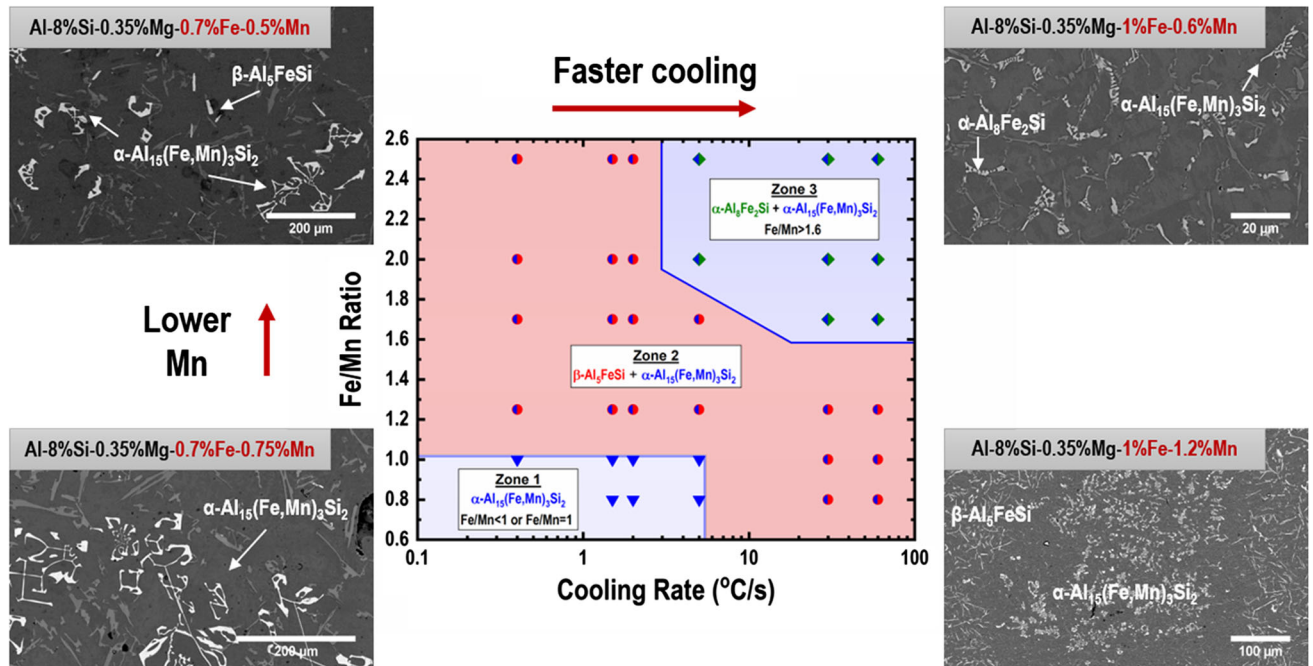


Fig. 9—The formation map of Fe-containing intermetallics in Al-Si-Mg casting alloys with high Fe content.

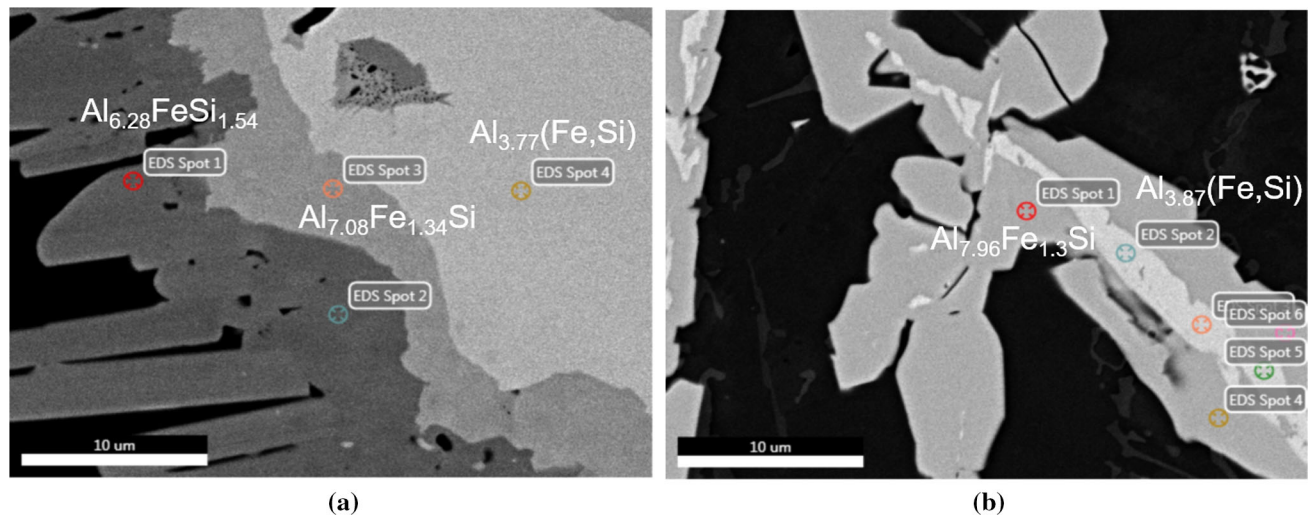


Fig. 10—The formation of Fe-rich intermetallics through peritectic reaction in Al-8 pct Si-10 pct Fe alloy: (a) 0.4 °C/s cooling rate; and (b) 30 °C/s cooling rate.

established Fe-to-Mn ratio of 2 may yield the desired microstructure in castings produced by HPDC or permanent mold casting processes, since the rapid cooling conditions can be sufficient to stop the peritectic transformation of $L + \alpha\text{-Al}_8\text{Fe}_2\text{Si} \rightarrow \beta\text{-Al}_5\text{FeSi}$ before its completion and yield microstructure that contains both $\alpha\text{-Al}_8\text{Fe}_2\text{Si}$ and $\alpha\text{-Al}_{15}(\text{Fe,Mn})_3\text{Si}_2$. However, there would be enough time for peritectic reaction to take place in castings produced with sand casting process and result in the formation $\beta\text{-Al}_5\text{FeSi}$ phase, if there is not enough Mn added to form the stable $\alpha\text{-Al}_{15}(\text{Fe,Mn})_3\text{Si}_2$ phase. Therefore, the required Mn content should be adjusted for different Fe concentrations and cooling

conditions to effectively avoid $\beta\text{-Al}_5\text{FeSi}$ phase in the as-cast microstructure.

IV. CONCLUSION

In summary, the cooling rate-dependent Fe-to-Mn ratios for recyclable Al-Si-Mg-based casting alloys with high Fe contents were determined through CALPHAD-assisted solidification experiments. By establishing the cooling rate dependency of the Fe-to-Mn ratio which suppresses $\beta\text{-Al}_5\text{FeSi}$ allows for increased use of secondary aluminum in casting

applications where mechanical properties (especially the ductility) are important. It was observed that, at low and intermediate cooling rates (such as gravity and low-pressure sand casting), an Fe-to-Mn ratio of ~ 1 is required to inhibit the detrimental β -Al₅FeSi phase formation and maintain the lowest possible Fe-rich intermetallic volume fraction in the as-cast microstructure. At high cooling rates (such as permanent mold casting and high-pressure die casting), however, Fe-to-Mn ratio higher than ~ 1.6 is required to obtain a mixture of compact metastable α -Al₈Fe₂Si and stable α -Al₁₅(Fe,Mn)₃Si₂ phases. The required Mn content decreases with increased cooling rate to avoid β -Al₅FeSi phase formation. By implementing this map, it is possible to optimize the microstructure to improve the mechanical properties, most notably the ductility, in recycled Al-Si-Mg alloys.

ACKNOWLEDGMENTS

The authors would like to acknowledge the National Science Foundation for supporting this work (Award CMMI-1432688). Dr. Yeou-Li Chu and Mr. Patrick Cheng of Ryobi Die Casting are also acknowledged for helpful discussions.

REFERENCES

1. A.I. Taub and A.A. Luo: *MRS Bull.*, 2015, vol. 40, pp. 1045–54.
2. J.G. Kaufman and E.L. Rooy: *Aluminum Alloy Castings: Properties, Processes, and Applications*, ASM International, Cleveland, 2004.
3. M.E. Schlesinger: *Aluminum Recycling*, 2nd ed., CRC Press, Boca Raton, FL, 2013.
4. W.J. Joost: *JOM*, 2012, vol. 64, pp. 1032–8.

5. G. Gaustad, E. Olivetti, and R. Kirchain: *Resour. Conserv. Recycl.*, 2012, vol. 58, pp. 79–87.
6. K. Nakajima, O. Takeda, T. Miki, K. Matsubae, S. Nakamura, and T. Nagasaka: *Environ. Sci. Technol.*, 2010, vol. 44, pp. 5594–5600.
7. A. Couture: *AFS Int. Cast Met. J.*, 1981, vol. 6, pp. 9–17.
8. P.N. Crepeau: *Trans. Am. Foundrymen's Soc.*, 1995, vol. 103, pp. 361–66.
9. J.A. Taylor: *Proc. Mater. Sci.*, 2012, vol. 1, pp. 19–33.
10. S. Terzi, J.A. Taylor, Y.H. Cho, L. Salvo, M. Suéry, E. Boller, and A.K. Dahle: *Acta Mater.*, 2010, vol. 58, pp. 5370–80.
11. C.M. Dinnis, J.A. Taylor, and A.K. Dahle: *Scr. Mater.*, 2005, vol. 53, pp. 955–58.
12. C. Puncrobutr, A.B. Phillion, J.L. Fife, P. Rockett, A.P. Horsfield, and P.D. Lee: *Acta Mater.*, 2014, vol. 79, pp. 292–303.
13. S. Seifeddine, S. Johansson, and I.L. Svensson: *Mater. Sci. Eng. A*, 2008, vol. 490, pp. 385–90.
14. J.Y. Hwang, H.W. Doty, and M.J. Kaufman: *Mater. Sci. Eng. A*, 2008, vol. 488, pp. 496–504.
15. D. Bösch, S. Pogatscher, M. Hummel, W. Fragner, P. Uggowitzer, M. Göken, and H. Höppel: *Metall. Mater. Trans. A*, 2015, vol. 46A, pp. 1035–45.
16. A. Gorny, J. Manickaraj, Z. Cai, and S. Shankar: *J. Alloys Compd.*, 2013, vol. 577, pp. 103–24.
17. Y. Awano and Y. Shimizu: *AFS Trans.*, 1990, vol. 98, pp. 889–95.
18. M.V. Kral: *Mater. Lett.*, 2005, vol. 59, pp. 2271–76.
19. L.A. Narayanan, F.H. Samuel, and J.E. Gruzleski: *Metall. Mater. Trans. A*, 1994, vol. 25A, pp. 1761–73.
20. C.M. Dinnis, J.A. Taylor, and A.K. Dahle: *Metall. Mater. Trans. A*, 2006, vol. 37A, pp. 3283–91.
21. S.G. Shabestari: *Mater. Sci. Eng. A*, 2004, vol. 383, pp. 289–98.
22. K. Liu, X. Cao, and X.G. Chen: *Metall. Mater. Trans. B*, 2012, vol. 43B, pp. 1231–40.
23. S. Ji, W. Yang, F. Gao, D. Watson, and Z. Fan: *Mater. Sci. Eng. A*, 2013, vol. 564, pp. 130–39.
24. R. Schmid-Fetzer and F. Zhang: *Calphad*, 2018, vol. 61, pp. 246–63.
25. X. Cao and J. Campbell: *Metall. Mater. Trans. A*, 2004, vol. 35A, pp. 1425–35.
26. N. Isono, P. Smith, D. Turnbull, and M.J. Aziz: *Metall. Mater. Trans. A*, 1996, vol. 27A, pp. 725–30.

Publisher's Note Springer Nature remains neutral with regard to jurisdictional claims in published maps and institutional affiliations.